CHAPTER 4

INFLUENCE OF MOLECULAR STRUCTURE, FLUORINATION AND CHAIN LENGTH ON THE DIELECTRIC PROPERTIES OF NEMATOGENIC BI-CYCLOHEXYL PHENYL DERIVATIVES

4.1 INTRODUCTION

Liquid crystal materials have many unique physical, optical and electro-optical properties and have received much attention in case of display applications and nematic liquid crystals are the most valuable in this regard. Nematic liquid crystals (NLCs) consist of anisotropic molecules that tend to align in a common local direction called the director which results in possessing several anisotropic properties like viscosity, elasticity, birefringence, dielectric permittivity, etc. In addition to this, NLCs have long-range orientational order, which gives rise to many properties important for LC displays [1–5]. Partially fluorinated phenyl-bicyclohexyl and biphenyl-cyclohexyl compounds are wide-range nematic materials characterised by low viscosity and high chemical stability, large dielectric anisotropy, low optical anisotropy and very good voltage holding ratio and they exhibit mesomorphism at ambient temperatures and have high bulk resistivity and low current consumption. These materials are, therefore, expected to be useful in making active matrix displays (AMDs) such as TFT (thin-film transistor) and MIM (metal–insulator–metal) systems [6-9]. These materials are also found to be useful in large information content display technology as well as for photonic applications [7-17]. Various physical properties of the compounds of this series have been investigated by many authors employing different experimental techniques like phase transitions and thermal properties [6, 18], optical birefringence [19], order parameter [12], viscosity [20], spectroscopic [21], dielectric, and elastic properties [14,22,23].

In this chapter dielectric behavior of six fluorinated bicyclohexyl compounds have been described which were studied in our laboratory by X-ray diffraction and optical birefringence methods [24,25].

Dielectric studies of liquid crystals have proven to be very useful as a source of information about specific intermolecular interactions, molecular associations, molecular dynamics and relaxation mechanisms, also important in the development of electro-optic devices [26-28]. The study of temperature dependence of the permittivity is also of considerable practical importance. The threshold voltage (V_{th}) and other operational parameters of liquid crystal display devices depend on the anisotropy of the permittivity ($\Delta\varepsilon$) [29] and the multiplexity of matrix displays may be limited by the temperature dependence of the permittivity. Due to frequency dependence of $\Delta\varepsilon$, V_{th} varies with frequency and causes the unfavorable problems on the display quality like lowered contrast, cross talk, etc. Understanding the factors that determine the

dielectric behaviour of liquid crystals will supplement the development of new materials with better display properties. So, the dielectric permittivities of liquid crystals have extensively been studied. Moreover, subject to an ac field, two non-collective molecular mode dielectric relaxations are observed in non-chiral low-molecular mass nematic liquid crystals. One is associated with rotation of the molecules around its short axis and the other occurs when the molecule rotates around its long axis. Other than positional ordering, reorientations of entire molecules around their short and long axes are one of the features that distinguish the liquid crystalline state from crystalline phase where these reorientations as well as intramolecular reorientations are usually frozen, and vibration of atoms about their equilibrium positions still persist. Therefore, information about the nature of molecular dynamics is possible to obtain from frequency and temperature dependent dielectric spectroscopic study [30–34].
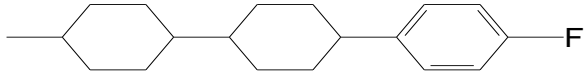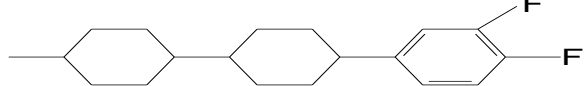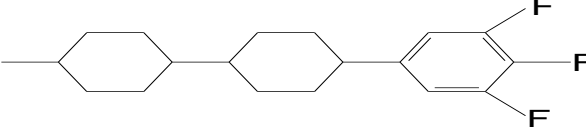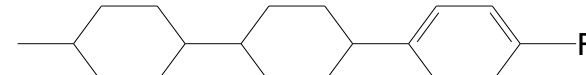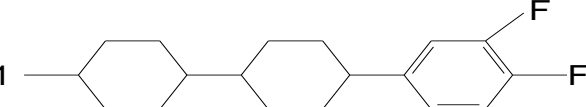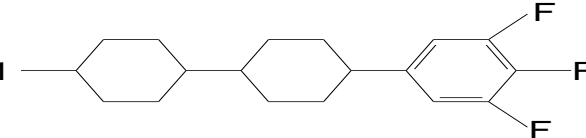
Results of crystal structure analysis of one of the compounds (5ccp-fff) have also been reported and an attempt has been made to find the effect of the molecular geometry and packing in the crystalline state on its phase behavior and different physical properties [35]. Crystal and molecular structures of related compounds 3ccp-ff and 3ccp-fff were reported from our laboratory before [36,37].

The compound 5ccp-fff is obtained by the introduction of one ethyl group to the chain of the compound 3ccp-fff and one ethyl group to the chain and one fluorine atom to the phenyl ring of 3ccp-ff. It is observed that transformation of 3ccp-fff to 5ccp-fff leads to the substantial increase of melting point and decrease of the nematogenic range [3ccp-fff: **Cr** 66.0 **N** 94.1 **I** and 5ccp-fff: **Cr** 88.0 **N** 102.4 **I**], and in case of transformation of 3ccp-ff to 5ccp-fff, change in the above thermal behaviour is more drastic [3ccp-ff: **Cr** 46.0 **N** 123.8 **I**]. In order to investigate how the molecular structure and packing of the three compounds differ in the crystalline state and their effect on observed phase behaviour, we have determined the crystal structure of 5ccp-fff. An excellent review on crystal structures of many liquid crystal compounds and their effect on mesogenic behaviour can be found in [38].

4.2 COMPOUNDS STUDIED

Molecular structures of the investigated fluorinated bicyclohexyl compounds along with their abbreviated names and transition temperatures (in $^{\circ}$C) are given in the Table 4.1. In the

Table 4.1: Molecular structures and transition temperatures of the studied compounds

Name	Molecular structure with transition temperature
4-propyl-4′-(4-fluorophenyl) bicyclohexane (3ccp-f)	C_3H_7 — (structure) — F **Cr 90.0 (71.0) N 158.0 I**
4-propyl-4′-(3, 4- difluoro-phenyl)bicyclohexane (3ccp-ff)	C_3H_7 — (structure) — F, F **Cr 45.6 N 123.8 I**
4-propyl-4′-(3,4, 5- trifluoro-phenyl)bicyclohexane (3ccp-fff)	C_3H_7 — (structure) — F, F, F **Cr 64.7 N 93.7 I**
4-pentyl-4′-(4-fluorophenyl) bicyclohexane (5ccp-f)	C_5H_{11} — (structure) — F **Cr 68.0 SmB 75.0 N 157.0 I**
4-pentyl-4′-(3, 4- difluoro-phenyl) bicyclohexane (5ccp-ff)	C_5H_{11} — (structure) — F, F **Cr 47.0 (26.8) N 125.2 I**
4- pentyl - 4′-(3,4,5-trifluoro-phenyl)bicyclohexane (5ccp-fff)	C_5H_{11} — (structure) — F, F, F **Cr 87.3 N 101.2 I**

abbreviated names the number at the beginning denotes the number of carbon atoms present in the alkyl chain, 'c' and 'p' represent respectively the cyclohexyl and phenyl ring in the core, f(s) denote the number of fluorine atoms in the terminal phenyl ring. All the investigated compounds exhibit nematic phase over a considerable temperature range, although the compound 5ccp-f shows, in addition, SmB phase within small temperature range, however, no studies have been made in that phase.

Table 4.2: Phase transition temperatures (^{0}C) of 3ccp-ff, 3ccp-fff and related compounds

Compound	Phase sequence
3ccp	Cr 76 SmB 97 N 103 I
3ccp-F	Cr 88.6 N 158.5 I
3ccp-Cl	Cr 75.1 Sm 79 N 192 I
3ccp-I	Cr 119 Sm 139.2 N 189.2 I
3ccp-CN	Cr 73.1 Sm 81.1 N 238.9 I
3ccp-ff	Cr 45.6 N 123.8 I
3ccp-fff	Cr 64.7 N 93.7 I
3ccp - OCF3	Cr 38.0 Sm 69.0 N 154 I
5ccp - C_3H_7	Cr 48.6 Sm 181 I
5cpp - C_3H_7	Cr 29 Sm 160 N 170 I

It is observed from the literature [9,39,40] that unsubstituted 4-phenyl-4-propyl-bicyclohexyl (3ccp) and para-substituted 3ccp, i.e. 3ccp-Cl, 3ccp-I and 3ccp-CN or para-substituted 5ccp-C_3H_7 and 5cpp-C_3H_7 exhibit both smectic and nematic phases, whereas mono-, di- and tri-substituted 3ccp exhibit only a nematic phase (Table 4.2). However, 3ccp-ff does not show mesogenity at all [39].

4.3 EXPERIMENTAL DETAILS

The phase behavior of the fluorinated bicyclohexyl compounds was studied using an optical polarizing microscope. Crystal and molecular structure was determined by direct methods. Static and frequency dependent dielectric properties was studied using computer controlled impedance analyzers HIOKI 3532-50 (50 Hz – 5 MHz) and HP 4192A (100 Hz –13 MHz). The elastic constants were measured by the Freédericksz transition technique [29]. The dipole-dipole correlation factor (g_λ) was determined following Bata and Buka [41]. Details of all the procedures have been described in chapter 2.

4.3.1 Structure Determination and Refinement

Crystal structure of only 5ccp-fff was determined as mentioned in the introduction. Crystals suitable for structure determination by X-rays were obtained from a mixture of dichloromethane and methyl alcohol by slow evaporation technique at room temperature. Transparent plate-shaped crystal (approximately 0.40 x 0.25 x 0.20 mm^3) was used for data collection on an CAD-4 diffractometer (Enraf-Nonius B.V., Rotterdam, The Netherlands) with graphite-monochromated CuKα radiation and ω-2θ scan. A total of 4112 unique reflections were measured within the range -6 $\leq$h $\leq$6, 0 $\leq$k 53, 0 $\leq$l $\leq$11. Of these, 2528 were above the significance level of 2.5 $\sigma(I_{obs})$ and were treated as observed. The range of (sin θ)/λ was 0.044-0.626Å (3.9 $\leq$ θ $\leq$74.7˚). Two reference reflections [(0 8 1), (1 2 1)] were measured hourly and showed no decrease during the 60-h collection time. Unit-cell parameters were refined by a least-squares fitting procedure using 23 reflections with 40.05 $\leq$ $\theta$$\leq$ 42.49°. Corrections for Lorentz and polarisation effects were applied. The structure was solved by the direct method program package CRUNCH [42]. Positions of the hydrogen atoms were calculated. Full-matrix least-squares refinement on F, anisotropic for the non-hydrogen atoms and isotropic for the hydrogen atoms, keeping the latter fixed at their calculated positions with an atomic displacement parameter (ADP) of U=0.15Å^2, converged to R=0.095, R$_w$ = 0.093, $(\Delta/\sigma)_{max}$=0.01, S=1.0. A weighting scheme W = $[2.5 + 0.01*\{\sigma(Fobs)\}^2 + 0.001/\{\sigma(Fobs)\}]^{-1}$ was used. A final difference Fourier map revealed a residual electron density between –0.38 and 0.37 eÅ^{-3}. Scattering factors were taken from Cromer and Mann and International Tables for X-ray Crystallography [43,44]. The anomalous scattering of F was taken into account [45]. All

calculations were performed with XTAL [46], unless stated otherwise. Supplementary tables and molecular picture were made with PLATON [47]. Important crystallographic data and refinement parameters are given in Table 4.3. The crystal structure has been deposited at the Cambridge Crystallographic Data Centre and allocated the deposition number CCDC 836063.

4.4 RESULTS AND DISCUSSIONS

4.4.1 Optimized Geometry Using Molecular Mechanics

To elucidate the structure of the investigated compounds, their optimized geometry was calculated using PM3 molecular mechanics method in Hyperchem software package [48]. Optimized lengths of the molecules, dipole moments and the corresponding moments of inertia values (along the three principal moments of inertia axes) are shown in the Table 4.4. It is observed that the dipole moment of the molecules increases as one move from f to ff to fff systems of a particular series, however increment is more in f to ff derivatives than in ff to fff derivatives. However no change in dipole moment is observed when the number of carbon atom in the chain increases. Such behavior has been reported before in nCHBT and nCB series [49-51], as discussed in chapter 3. Previously reported theoretical values for 3ccp-ff are 3.32D [7] and 3.2D [14]. Thus the value obtained from our calculation (3.21 D) agrees with that reported by Klasen et al. [14]. Molecular conformation in optimized geometry has been compared with that obtained from crystal structure analysis in the next section.

Table 4.3: Important Crystallographic data

Formula	$C_{23}H_{33}F_3$
Formula Weight	366.49g/mol
T (K)	293(2)
Radiation, λ (CuKα)	1.54180 Å
Crystal System	monoclinic
Space group	P21/n
a	4.9860(9)Å
b	42.875(5) Å
c	9.623(3) Å
β	92.08(2)°
V	2055.8(8)Å^3
Z	4
D_{cal}	1.184g/cc
F(000)	792
Crystal Size	0.4 0x 0.25x 0.20 mm^3
Independent reflections	4112
No. of observed reflections	2528 [I>2.5σ(I)]
Refinement method	full-matrix least-squares on F
R (Observed reflection)	0.095
R_W (Observed reflection)	0.093

Table 4.4: Optimized length, dipole moment and moment of inertia of the investigated compounds

Compound	Optimized Length (Å)	Dipole Moment (Debye)	Moment of Inertia ($\times 10^{-46}$ Kg m^2)		
			I_{XX}	I_{YY}	I_{ZZ}
3ccp-f	17.01	1.93	383.40	7024.29	7106.98
3ccp-ff	17.02	3.21	440.27	7298.36	7954.52
3ccp-fff	17.02	3.72	580.69	8457.54	8573.88
5ccp-f	19.38	1.93	426.42	9503.92	9568.43
5ccp-ff	19.38	3.12	519.99	10342.2	10477.9
5ccp-fff	19.46	3.77	675.42	11574.4	11678.6

4.4.2 Three-Dimensional Crystal Structure Determination

Figure 4.1 represents the molecular structure and the atom numbering schemes of non-hydrogen atoms. Final positional coordinates with equivalent isotropic thermal parameters, anisotropic thermal parameters, bond lengths and bond angles of the non-hydrogen atoms are listed in Tables 4.5 – 4.9. The average aromatic bond length and bond angle of the phenyl ring are found to be 1.368 (9) Å and 120.0 (6)^0, consistent with corresponding values in 3ccp-ff and 3ccp-fff which are 1.377 (6) Å and 120.0 (4)^0 and 1.368(6) Å and 120.0 (4)^0 respectively. These values are also in agreement with the geometry of the other phenyl moieties reported in literature [52–54]. The cyclohexyl groups are in chair conformation as was observed in 3ccpff, 3ccp-fff and other mesogenic molecules [55-57]. The alkyl chain is in all-*trans* conformation with mean bond distance of 1.509(9) Å and bond angle 114.7(6)^0 as found in other mesogenic compounds [58-60]. These values are in good agreement with the corresponding values in 3ccp-ff and 3ccp-fff 1.519(8) Å and 113.7(5)^0, and 1.520(6) Å and 111.6 (4)^0. Bond lengths of C1–F1, C2–F2 and C6–F3 are found to be 1.378(7)Å, 1.361(8) Å and 1.352(8) Å close to the values observed in 3ccp-ff [1.351(4) Å, 1.353(5) Å] and in 3ccp-fff [1.344(5) Å, 1.354(4) Å and 1.354(5) Å] and in other fluorophenyl compounds 1.347(3) Å in reference [61] and 1.363(4) Å in reference [62]. Thus it may be inferred that the bond lengths and angles of 5ccp-fff is similar to 3ccp-ff and 3ccp-fff and to other mesogenic molecules.
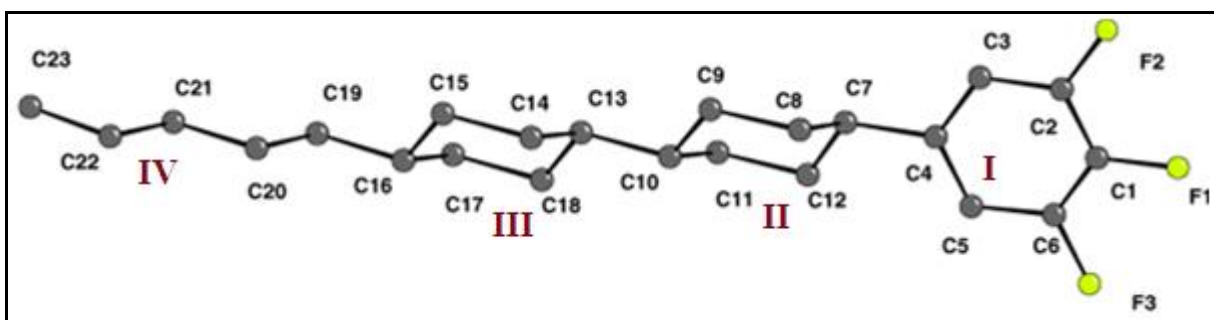

Figure 4.1: A perspective view of 5ccp-fff molecule with atom numbering scheme. Meaning of figures I-IV has been discussed in the text

Geometry of the 5ccp-fff molecule may be described in terms of four planes of the phenyl ring (**I**), the two cyclohexyl rings (**II** and **III**) and the plane of the alkyl chain (**IV**), as shown in Figure 4.1. The phenyl ring is highly planar and the three fluorine atoms are almost in the same

plane. Almost similar phenyl ring geometry was observed in 3ccp-ff and 3ccp-fff. The dihedral angles between the planes (**I** and **II**), (**I** and **III**), (**I** and **IV**), (**II** and **III**), (**II** and **IV**) and (**III** and **IV**) are 47.2^0, 68.7^0, 91.7^0, 22.5^0, 44.7^0 and 23.0^0 respectively. The corresponding angles are 83.2^0, 83.4^0, 51.3^0, 0.8^0, 35.9^0 and 36.4^0 in 3ccp-fff and, 122.1^0, 123.5^0, 8.8^0, 3.4^0, 127.8^0 and 128.7^0 in 3ccp-ff respectively. Thus, in 3ccp-fff and 3ccp-ff, the dihedral angles between the two cyclohexyl groups were found to be 0.8^0 and 3.4^0 respectively compared to 22.5^0 in this case. The phenyl ring and the pentyl chain are at right angle (dihedral angle 91.7^0) in 5ccp-fff whereas they were at an angle 51.3^0 in 3ccp-fff and 8.8^0 in 3ccp-ff respectively. Dihedral angles between the phenyl and nearby cyclohexyl ring is found to be 47.2^0 in 5ccp-fff, where the values were 83.2^0 in 3ccp-fff and 122.1^0 in 3ccp-ff respectively. Thus it is observed that molecular conformation of 5ccp-fff is quite different from those of 3ccp-fff and 3ccp-ff systems, although their bond lengths and angles are quite similar.

Table 4.5: Fractional co-ordinates and equivalent isotropic thermal parameters of the non-Hydrogen atoms with e.s.d's in parentheses of 5ccp-fff

Atom	X	Y	Z	U_{eq} (Å^2)
F1	-0.0988(8)	0.44143(8)	0.3107(5)	0.0917(16)
F2	0.3085(9)	0.47200(10)	0.4424(5)	0.108(2)
F3	-0.4128(9)	0.47212(9)	0.1217(5)	0.0979(19)
C1	-0.0554(13)	0.47246(13)	0.2820(7)	0.058(2)
C2	0.1475(13)	0.48755(15)	0.3485(7)	0.066(2)
C3	0.1955(13)	0.51910(14)	0.3225(7)	0.068(3)
C4	0.0358(12)	0.53428(13)	0.2252(6)	0.0530(19)
C5	-0.1678(13)	0.51900(14)	0.1557(7)	0.062(2)
C6	-0.2083(13)	0.48733(14)	0.1883(7)	0.061(2)
C7	0.0938(12)	0.56910(13)	0.1967(7)	0.061(2)
C8	-0.0011(16)	0.58942(14)	0.3135(7)	0.078(3)
C9	0.0758(17)	0.62408(15)	0.2917(7)	0.080(3)
C10	-0.0190(12)	0.63688(13)	0.1530(6)	0.056(2)
C11	0.0647(16)	0.61570(15)	0.0364(7)	0.080(3)
C12	-0.0191(16)	0.58102(14)	0.0611(7)	0.078(3)
C13	0.0721(12)	0.67115(13)	0.1291(6)	0.054(2)
C14	-0.0137(15)	0.69319(14)	0.2438(7)	0.073(2)
C15	0.0760(14)	0.72708(13)	0.2182(7)	0.069(2)
C16	-0.0153(12)	0.73956(13)	0.0790(6)	0.057(2)
C17	0.0718(15)	0.71773(14)	-0.0341(7)	0.071(2)
C18	-0.0219(14)	068352(14)	-0.0109(7)	0.067(3)
C19	0.0869(13)	0.77282(13)	0.0511(7)	0.063(2)
C20	-0.0196(13)	0.79844(15)	0.1410(7)	0.071(3)
C21	0.0856(14)	0.83021(14)	0.1047(8)	0.072(3)
C22	-0.0195(15)	0.85694(16)	0.1927(9)	0.087(3)
C23	0.0952(19)	0.88741(17)	0.1604(11)	0.114(4)

Table 4.6: Anisotropic thermal parameters of the non-Hydrogen atoms with the e.s.d's in parentheses

The temperature factor is of the form

exp $[2\pi^2 (U_{11}h^2a*^2+U_{22}k^2b*^2+U_{33}l^2c*^2+2U_{12}hka*b*+2U_{13}hla*c*+2U_{23}klb*c*]$

Atom	U_{11}	U_{22}	U_{33}	U_{23}	U_{13}	U_{12}
F1	0.101(3)	0.051(2)	0.123(3)	0.015(2)	0.003(3)	-0.002(2)
F2	0.118(4)	0.070(3)	0.133(4)	0.026(3)	-0.043(3)	0.003(3)
F3	0.098(3)	0.064(3)	0.129(4)	-0.010(2)	-0.033(3)	-0.012(2)
C1	0.063(4)	0.040(3)	0.072(4)	-0.002(3)	0.003(3)	-0.001(3)
C2	0.066(4)	0.057(4)	0.075(4)	0.011(3)	-0.014(4)	0.010(3)
C3	0.072(4)	0.050(4)	0.080(5)	0.004(3)	-0.003(4)	-0.001(3)
C4	0.052(3)	0.047(3)	0.060(4)	0.001(3)	0.001(3)	0.008(3)
C5	0.065(4)	0.051(4)	0.070(4)	-0.003(3)	-0.006(3)	0.007(3)
C6	0.062(4)	0.049(3)	0.071(4)	-0.010(3)	-0.011(3)	0.001(3)
C7	0.059(4)	0.051(3)	0.072(4)	-0.002(3)	0.007(3)	0.004(3)
C8	0.122(6)	0.048(4)	0.063(4)	0.003(3)	0.006(4)	-0.006(4)
C9	0.124(6)	0.052(4)	0.064(4)	0.001(3)	-0.001(4)	-0.009(4)
C10	0.062(4)	0.045(3)	0.061(4)	0.001(3)	0.007(3)	0.005(3)
C11	0.122(6)	0.049(4)	0.071(5)	-0.003(3)	0.021(4)	0.008(4)
C12	0.127(6)	0.045(4)	0.063(4)	-0.004(3)	-0.001(4)	0.010(4)
C13	0.062(4)	0.044(3)	0.056(4)	-0.002(3)	0.007(3)	0.001(3)
C14	0.103(5)	0.049(3)	0.068(4)	-0.004(3)	0.020(4)	-0.003(4)
C15	0.096(5)	0.042(3)	0.069(4)	-0.004(3)	0.014(4)	-0.003(3)
C16	0.061(4)	0.049(3)	0.062(4)	0.003(3)	0.012(3)	0.002(3)
C17	0.100(5)	0.048(3)	0.065(4)	0.004(3)	0.013(4)	0.005(3)
C18	0.090(5)	0.049(4)	0.062(4)	0.002(3)	0.004(4)	0.002(3)
C19	0.075(4)	0.038(3)	0.078(4)	0.000(3)	0.016(4)	-0.001(3)
C20	0.069(4)	0.059(4)	0.086(5)	-0.005(3)	0.022(4)	-0.003(3)
C21	0.082(5)	0.041(3)	0.095(5)	0.001(3)	0.016(4)	-0.002(3)
C22	0.087(5)	0.055(4)	0.119(6)	-0.002(4)	0.024(5)	0.003(4)
C23	0.125(7)	0.049(4)	0.168(9)	-0.007(5)	0.012(7)	0.002(5)

Table 4.7: Bond lengths (Å) of the non-Hydrogen atoms

with standard deviations in parentheses

Atom	Atom	Bond Length	Atom	Atom	Bond Length
F1	C1	1.378(7)	C10	C11	1.514(9)
F2	C2	1.361(8)	C10	C13	1.558(8)
F3	C6	1.352(8)	C11	C12	1.565(9)
C1	C2	1.343(9)	C13	C14	1.526(9)
C1	C6	1.323(9)	C13	C18	1.507(9)
C2	C3	1.398(9)	C14	C15	1.543(8)
C3	C4	1.371(9)	C15	C16	1.498(9)
C4	C5	1.363(9)	C16	C17	1.511(9)
C4	C7	1.547(8)	C16	C19	1.541(8)
C5	C6	1.410(9)	C17	C18	1.558(9)
C7	C8	1.512(9)	C19	C20	1.507(9)
C7	C12	1.493(9)	C20	C21	1.505(9)
C8	C9	1.551(9)	C21	C22	1.529(10)
C9	C10	1.503(9)	C22	C23	1.464(11)

Table 4.8: Bond angles (º) involving non-Hydrogen atoms

with standard deviations in parentheses

Atom	Atom	Atom	Angle	Atom	Atom	Atom	Angle
F1	C1	C2	119.4(6)	C9	C10	C11	11.7(5)
F1	C1	C6	120.7(6)	C9	C10	C13	113.1(5)
C2	C1	C6	119.9(6)	C11	C10	C13	111.5(5)
F2	C2	C1	119.7(6)	C10	C11	C12	112.0(5)
F2	C2	C3	119.5(6)	C7	C12	C11	111.3(5)
C1	C2	C3	120.8(6)	C10	C13	C14	112.7(5)
C2	C3	C4	118.9(6)	C10	C13	C18	112.4(5)
C3	C4	C5	120.7(5)	C14	C13	C18	110.0(5)
C3	C4	C7	118.1(5)	C13	C14	C15	112.2(5)
C5	C4	C7	121.2(5)	C14	C15	C16	113.5(5)
C4	C5	C6	117.6(6)	C15	C16	C17	109.7(5)
F3	C6	C1	119.8(5)	C15	C16	C19	113.2(5)
F3	C6	C5	118.1(6)	C17	C16	C19	110.0(5)
C1	C6	C5	122.2(6)	C16	C17	C18	112.6(5)
C4	C7	C8	111.0(5)	C13	C18	C17	112.0(5)
C4	C7	C12	114.7(5)	C16	C19	C20	116.7(5)
C8	C7	C12	109.5(5)	C19	C20	C21	113.2(6)
C7	C8	C9	111.5(6)	C20	C21	C22	114.9(6)
C8	C9	C10	113.5(6)	C21	C22	C23	114.0(7)

Length of the 5ccp-fff molecule in the crystalline state is found to be 19.85 Å [F1-H233], whereas the model length in the most extended conformation is 20.14 Å. Thus, the molecules are almost in the most extended conformation as was observed in 3ccp-fff and 3ccp-ff.

Packing of the molecules in the unit cell is shown in Figure 4.2, which shows that the molecules run almost parallel to each other but not parallel to any crystallographic axis as was seen in 3ccp-fff and 3ccp-ff systems. To describe the nature of packing, the direction cosines of the molecular long axis, defined as the best fitted line through all the non-H atoms, have been calculated and are found to be 0.4197, 0.8928 and 0.1637. In other words, the molecules are inclined to the orthogonal X, Y and Z axes at angles 65.2^0, 26.8^0 and 80.6^0 respectively. The corresponding angles are 67.5^0, 121.5^0 and 40.4^0 in case of 3ccp-fff and 75.95^0, 99.0^0 and 16.8^0 in 3ccp-ff.
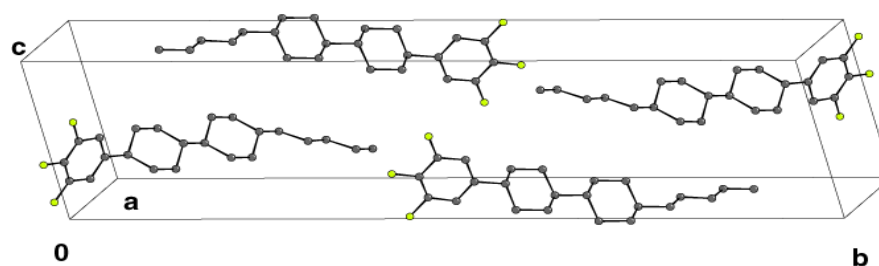
Figure 4.2: Partial packing of 5ccp-fff molecule in the crystallographic unit cell

Projections of the crystal structure along the crystallagraphic axes **a** and **c** are shown in Figure 4.3 and Figure 4.4, respectively. It is evident that the molecules are packed with various degrees of overlapping with the neighbouring ones. Orientation of the molecules in adjacent layers is opposite to each other. Overlaps of the molecules in the neighbouring layers are in the phenyl-phenyl groups in one side and in the cyclohexyl-alkyl chain part on the other side. Similar type of overlapping has been found for the compounds 3ccp-fff and 3ccp-ff. This type of imbricated mode of packing is usually observed in crystalline phase as a precursor to nematic phase [15,58].
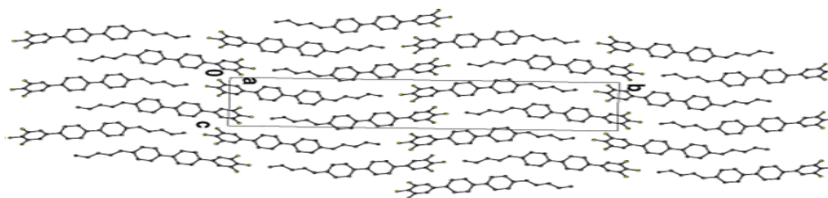
Figure 4.3: Crystal structure of 5ccp-fff projected along *a*-axis.
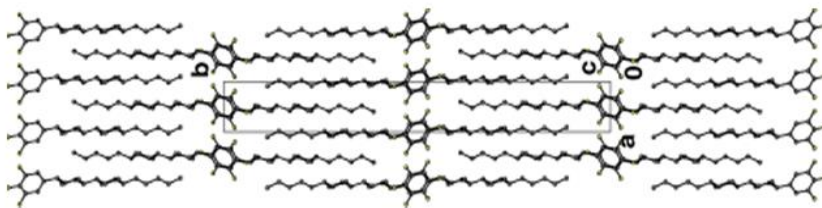
Figure 4.4: Crystal structure of 5ccp-fff projected along *c*-axis.

Intermolecular distances between the neighbouring molecules were calculated and several van der Waals interactions were observed. Selected intermolecular distances, less than 4.0 Å, are shown in Table 4.9.

Table 4.9: Selected intermolecular short contact distances less than 4.0 Å of 5ccp-fff

Atom	Atom	Distance	Atom	Atom	Distance
F1	F2(a)	3.511	F3	C6(b)	3.884
F3	F2(a)	3.429	F3	C12(b)	3.993
F3	C1(a)	3.606	C5	F3(b)	3.352
F3	C2(a)	3.218	C6	F3(b)	3.884
F3	C3(a)	3.446	C12	F3(b)	3.993
F3	C4(a)	3.981	F1	C23(c)	3.549
C1	F2(a)	3.577	F2	C23(c)	3.821
C5	C3(a)	3.609	C8	C23(d)	3.997
C6	F2(a)	3.555	C14	C19(d)	3.818
C6	C2(a)	3.613	C15	C19(d)	3.992
F3	F3(b)	3.436	C20	C17(d)	3.764
F3	C5(b)	3.352			

Subscripted atoms are at (a) x-1, y, z (b) –x-1, - y+1, -z

(c) –x-1/2 , -y-1/2 , -z+1/2 (d) –x-1/2, -y+3/2, z+1/2

Four different types of molecular overlaps are observed between neighbouring molecules as shown in Figure 4.5: (i) pair of parallel molecules in head-to-head configuration overlaps completely (related by symmetry operation '**a**' having pair length 20.31 Å), (ii) pair of antiparallel molecules in head-to-tail configuration overlaps partially (related by symmetry operation **'b'** having associated length 35.23 Å), (iii) pair of parallel molecules in head-to-head configuration with no overlap (related by symmetry operation '**c**' having associated length 41.36 Å and (iv) pair of antiparallel molecules in head-to-tail configuration overlaps partially in the alkyl cyclohexyl group (related by symmetry operation '**d**' having associated length 27.03 Å).
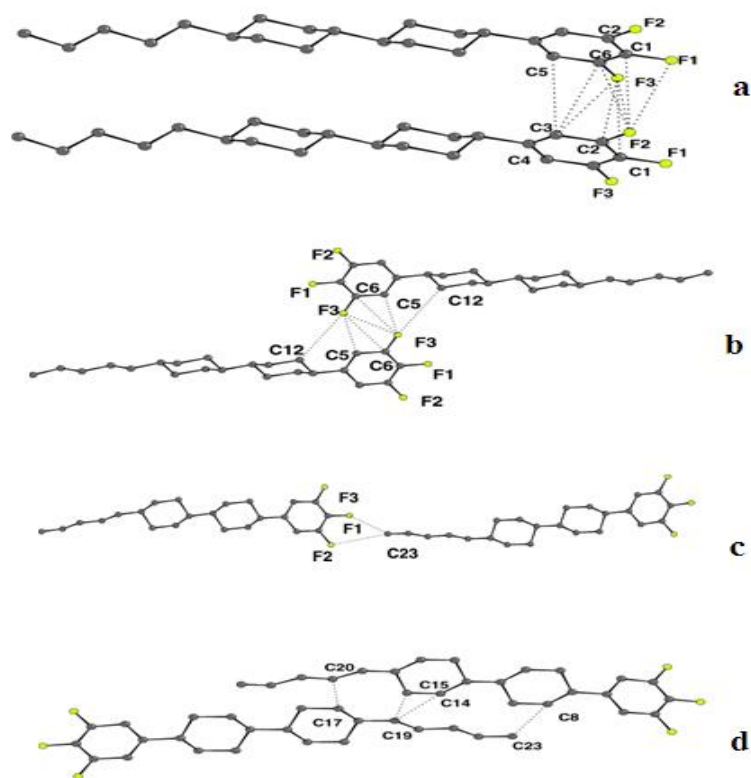
Figure 4.5: Different types of molecular associations observed in the crystal structure of 5ccp-fff. Values of the relevant inter atomic distances and meaning of the symmetry relations (a), (b), (c) and (d) are given in Table 4.9

As noted before, a preliminary molecular modelling calculation was made using the semi-empirical PM3 method and almost similar molecular conformation with molecular length of 19.46 Å was obtained when the geometry of the molecule was optimised assuming it as if in

vacuo. A single point energy calculation on an isolated molecule, as extracted from the crystal data, yields a dipole moment (μ) of 3.77 D with direction cosines 0.26, 0.95 and –0.17. Optimised geometry also results in same dipole moment with same direction cosines. But in case of 3ccp-ff and 3ccp-fff, the values are not same. In 3ccp-ff, single point energy calculation on crystal data and optimised geometry revealed slightly different dipole moments (3.54 D and 3.21 D) and in 3ccp-fff the values are 3.61 D and 3.72 D, respectively. Moreover, dipole moments, estimated from optimised geometry, are inclined at angles 18°, 17° and 43° with the molecular long axes in 5ccp-fff, 3ccp-fff and 3ccp-ff, respectively. Thus, conformation of 5ccp-fff in vacuo and in crystalline state appears to be same whereas they differ in two states in both 3ccp-ff and 3ccp-fff.

Calculated density in the crystalline state of 5ccp-fff is found to be slightly less (1.184 g/cc) than in 3ccp-fff (1.19 g/cc). Measured density in the nematic state was also less in 5ccp-fff (0.98 g/cc) than in 3ccpfff (1.08 g/cc) (near **Cr–N** transition point) [24]. Thus, 5ccp-fff molecules are more efficiently packed in both crystalline and nematic phases compared to 3ccp-fff. This explains that 5ccp-fff has higher melting point than that of 3ccp-fff. From small-angle X-ray diffraction study on magnetically aligned samples, average intermolecular distance (D) and apparent molecular length (l) were also measured in our laboratory [63]. Observed D values were found to be slightly more in 5ccp-fff (5.64 Å) than in 3ccp-fff (5.55 Å) and 3ccp-ff (5.35 Å) near **Cr–N** transition temperature. Apparent lengths of the molecules were found to be 27.1 Å, 24.9 Å and 22.8 Å, respectively, in 5ccp-fff, 3ccp-fff and 3ccp-ff systems. It is observed that in each case the apparent molecular length (l) is more than the model length obtained from most extended conformation. Thus, there exist some sort of bimolecular associations in all three molecular systems. This type of molecular association was observed in the isothiocyanato systems described in chapter 3 and was also reported in nematogenic 5CB and 7CB [64] and later found in other systems [60,65].

4.4.3 Static Dielectric Study

Principal dielectric constants ($\varepsilon_\parallel$ and $\varepsilon_\perp$) of all the six compounds were measured at 10 kHz in planar (HG) cell. In order to determine switching voltage required to switch molecular alignment from planar (*HG*) to homeotropic (*HT*) configuration, dielectric permittivity was

measured as a function of DC bias voltage across the cell and results are shown in the Figure 4.6 – 4.11. Values of threshold voltage (V_{th}), driving voltage (V_d) and driving field for the six compounds are listed in Table 4.10.

Table 4.10: Threshold voltage, driving voltage and driving field of the compounds

Compounds	Threshold Voltage (V_{th}) (Volt)	Driving Voltage (V_d) (Volt)	Driving Field ($V\mu m^{-1}$)
3ccp-f	2.57	9.07	1.71
3ccp-ff	1.61	8.08	1.52
3ccp-fff	1.02	6.12	1.20
5ccp-f	2.73	10.0	1.96
5ccp-ff	2.27	8.48	2.22
5ccp-fff	1.1	5.0	1.05

It is clear from the above table that, as number of fluorine increases threshold voltage as well as driving voltage decrease considerably in both the series (3ccp series & 5ccp series) while with increasing chain length V_{th} and V_d increases slightly except in triply fluorinated compound. In other words, increase of chain length by two carbon atoms has less effect on switching property compared to increased lateral fluorination. Similar behavior was also observed in isothiocyanato compounds as described in chapter 3. It is further observed, comparing data in Tables 3.3 and 4.10, that threshold voltage in these compounds are considerably less than that observed in the laterally fluoro-substituted terphenyl-based isothiocyanato compounds (2TP-3'F-4NCS, 2TP-3',3F-4NCS and 4TP-3',3F-4NCS). This is may be due to the replacement of two phenyl groups by more flexible cyclohexyl groups and the bulky isothiocyanato group by small fluoro group. However, driving field for all the compounds is suitable for thin ($< 2\mu m$) TFT based LC display

cells. Nevertheless, $5V\mu m^{-1}$ field was used for switching from HG to HT configuration while measuring $\varepsilon_\parallel$ and $\varepsilon_\perp$.
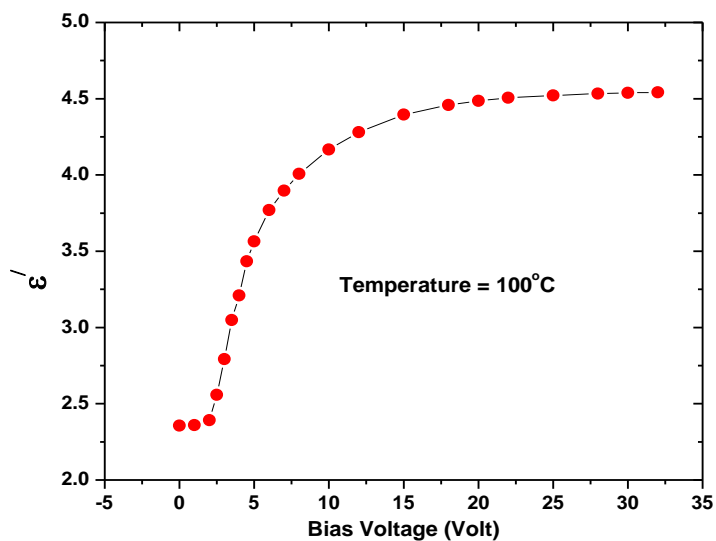
Figure 4.6: Real part of dielectric constant (ε') as a function of bias voltage at 10 kHz in 3ccp-f
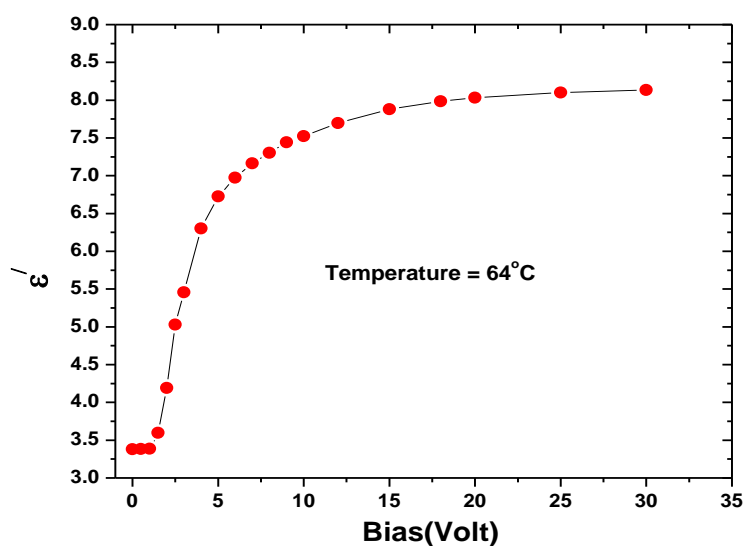
Figure 4.7: Real part of dielectric constant (ε') as a function of bias voltage at 10 kHz in 3ccp-ff
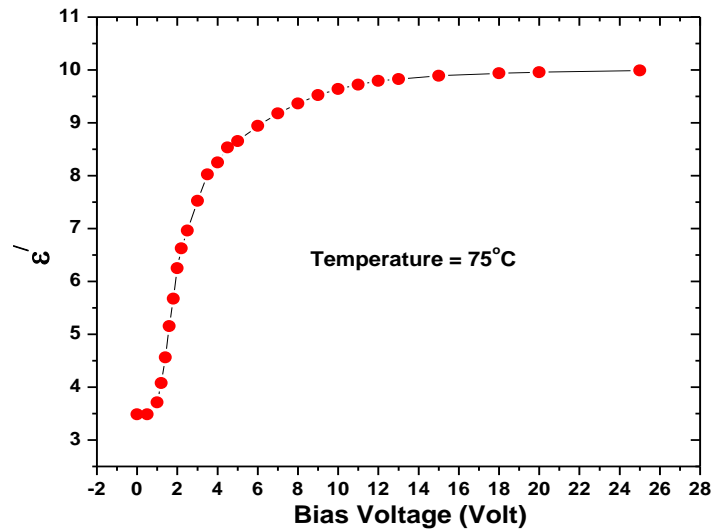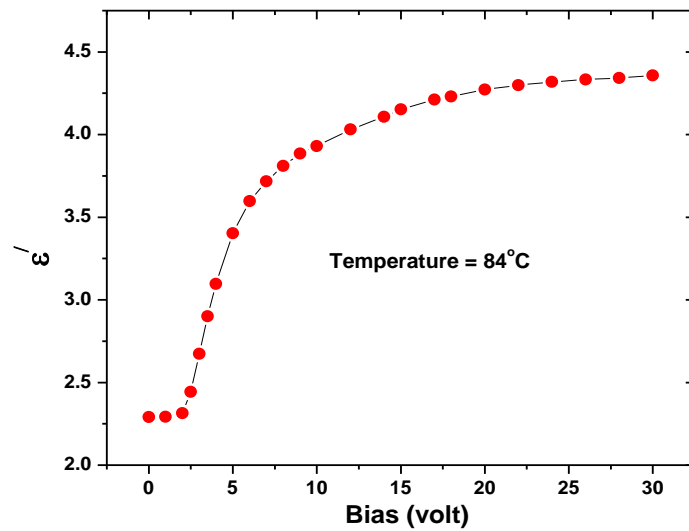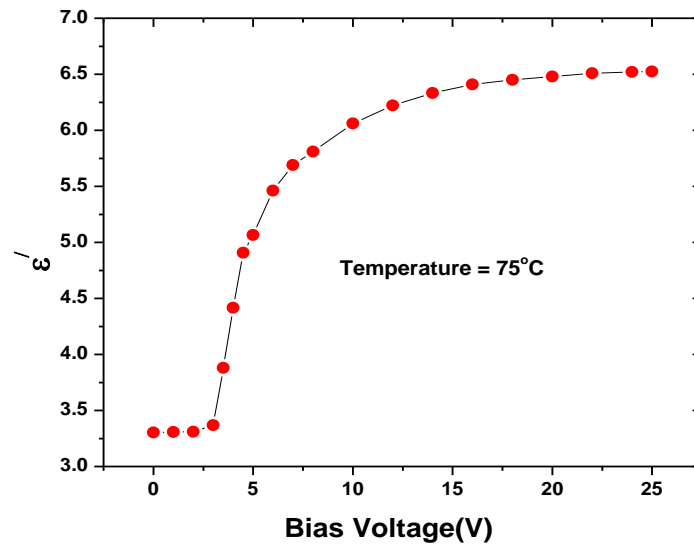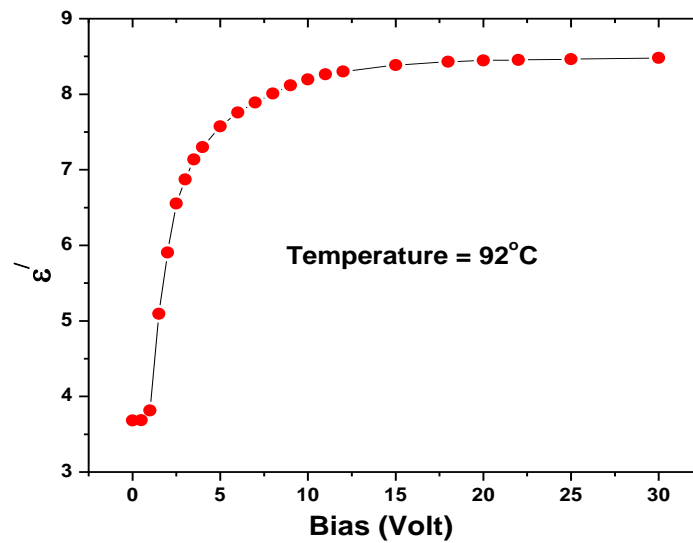
Figure 4.8: Real part of dielectric constant ($\varepsilon^{/}$) as a function of bias voltage at 10 kHz in 3ccp-fff

Figure 4.9: Real part of dielectric constant ($\varepsilon^{/}$) as a function of bias voltage at 10 kHz in 5ccp-f

Figure 4.10: Real part of dielectric constant (ε') as a function of bias voltage at 10 kHz in 5ccp-ff

Figure 4.11: Real part of dielectric constant (ε') as a function of bias voltage at 10 kHz in 5ccp-fff

Dielectric constants parallel ($\varepsilon_\parallel$) and perpendicular ($\varepsilon_\perp$) to molecular axis, their average value ε_{av}, in nematic phase and value in isotropic phase (ε_{iso}) have been determined as a function of temperature. Variations of principal dielectric constants with temperature are shown in Figures 4.12 – 4.17. Since the molecules possess quite strong axial dipole moment, value of dielectric constants parallel to molecular axis is found to be large compared to component perpendicular to the molecular axis. It is not clear why in 5ccp-f and 5ccp-ff systems $\varepsilon_\parallel$ approaches quite fast to $\varepsilon_\perp$ far away from T_{NI}. Average value of the dielectric constant is found to be slightly less than the extrapolated values of ε_{iso} in all cases [labeled as $(\varepsilon_{iso})_{ext}$ in the figures]. Similar difference has been observed in systems having strong axial moments [66-68]. In contrary, nonpolar molecules like di-alkyl azobenzenes do not show such discontinuity [32]. This has been explained assuming the presence of short-range antiparallel order in the nematic state [36,69].
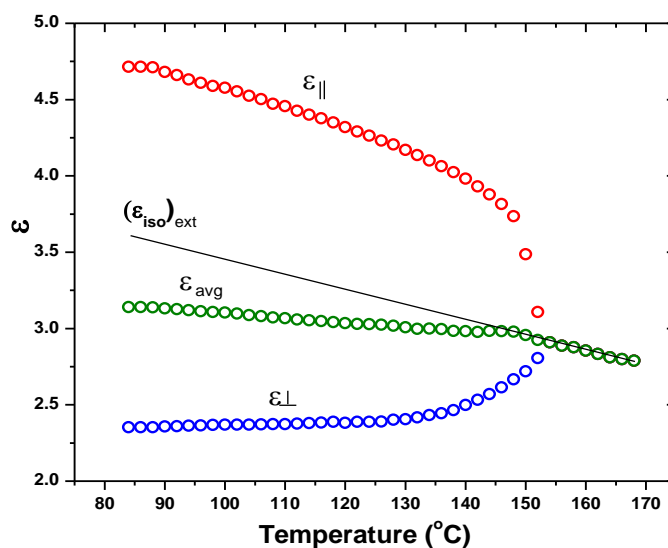
Figure 4.12: Temperature dependence of dielectric permittivity of compound 3ccp-f
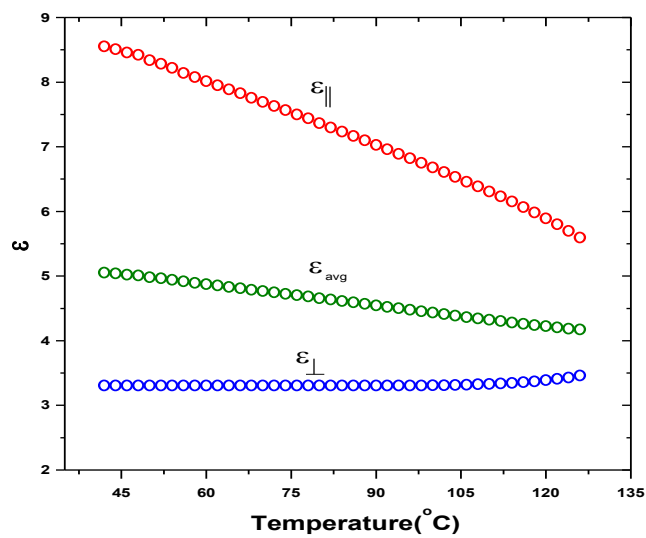
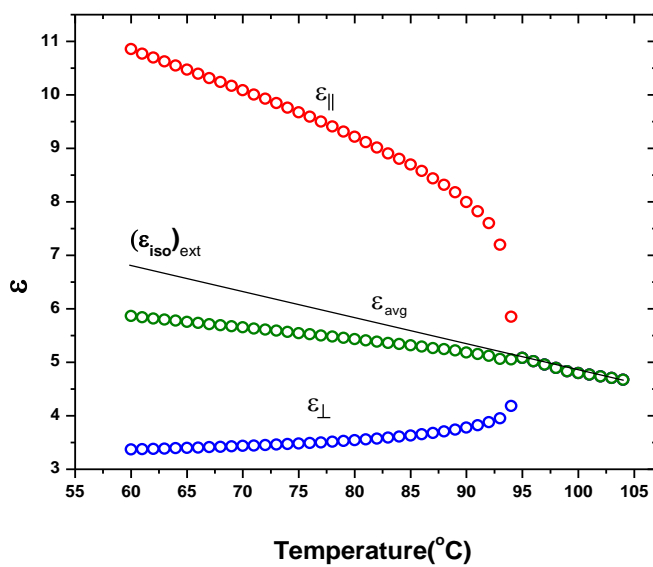Figure 4.13: Temperature dependence of dielectric permittivity of compound 3ccp-ff

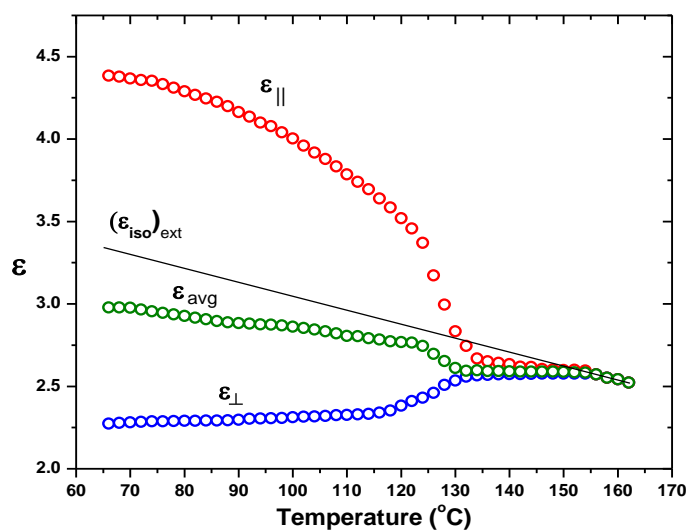Figure 4.14: Temperature dependence of dielectric permittivity of compound 3ccp-fff

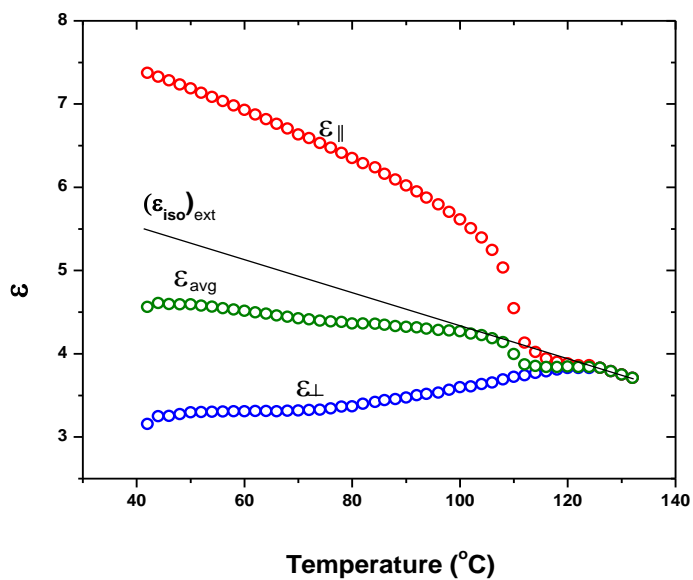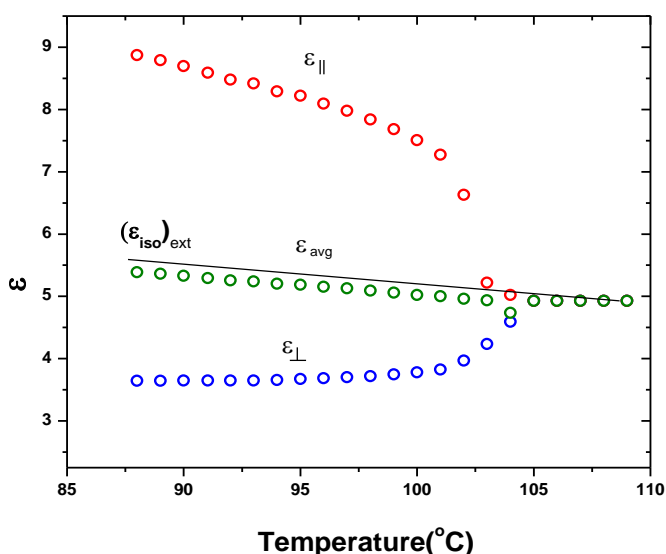Figure 4.15: Temperature dependence of dielectric permittivity of compound 5ccp-f

Figure 4.16: Temperature dependence of dielectric permittivity of compound 5ccp-ff

Figure 4.17: Temperature dependence of dielectric permittivity of compound 5ccp-fff

Temperature dependence of dielectric anisotropy ($\Delta\varepsilon = \varepsilon_\parallel - \varepsilon_\perp$) for all the compounds is shown in Figure 4.18. It is found to be positive in all and also decreases with temperature. The highest $\Delta\varepsilon$ values near crystal to nematic transition are found to be 2.36, 5.25, 7.48 in 3ccp-f, 3ccp-ff and 3ccp-fff respectively and that in 5ccp series are 2.12, 4.22 and 6.46 respectively. It is clear that increased fluoro substitution causes increased dielectric anisotropy as observed in terphenyl compounds in chapter 3. However, unlike in terphenyl compounds, increased chain length causes slightly decreased $\Delta\varepsilon$ in these compounds. Moreover, $\Delta\varepsilon$ in this case is very less than that observed in terphenyl-based isothiocyanato nematic compounds, described in chapter 3. This is expected since dipole moment of fluorobenzene is 1.50 D while that of isothiocyanato group is 3.7 D.
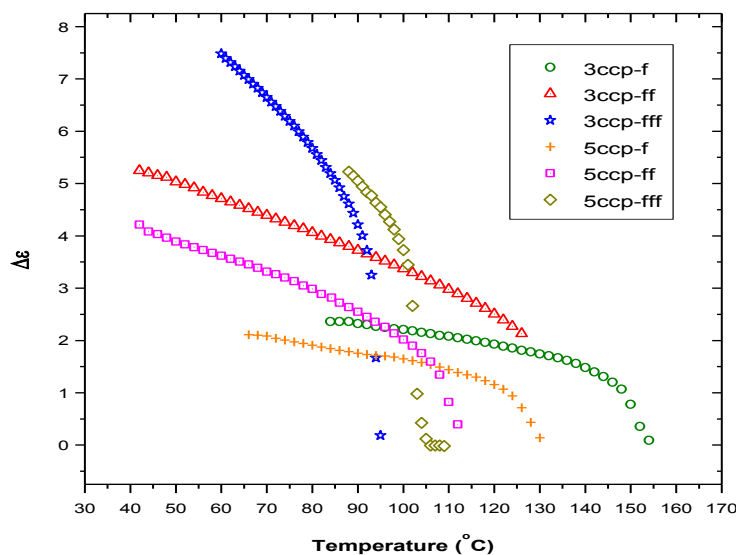
Figure 4.18: Temperature dependence of dielectric anisotropy ($\Delta\varepsilon$) of the compounds

The splay elastic constant (K_{11}), is found to exhibit similar decreasing trend with temperature as observed in dielectric anisotropy and is shown in Figure 4.19. It is noted that K_{11} near melting point for the compounds 3ccp-f and 5ccp-f are 13.9 x 10^{-12} N, 14.1 x 10^{-12} N; for 3ccp-ff and 5ccp-ff are 0.122 x 10^{-10} N, 11.2 x 10^{-12} N and for 3ccp-fff and 5ccp-fff are 6.9 x 10^{-12} N, 5.6 x 10^{-12} N. Thus with increased fluorination K_{11} decreases, becomes almost half in case of single to triple fluoro substitution, but with chain length very small unsystematic change is observed. Thus fluorination and chain length dependence of K_{11} is different from terphenyl based compounds as discussed in chapter 3. K_{11} of the present compounds are also much less than that observed in terphenyl-based isothiocyanato nematic compounds. This is probably due to the replacement of two phenyl groups by more flexible cyclohexyl groups and the bulky isothiocyanato group by small fluoro group. Since switching time is inversely proportional to K_{11}, faster response is expected in triply fluorinated compounds than the singly and doubly fluorinated compounds.
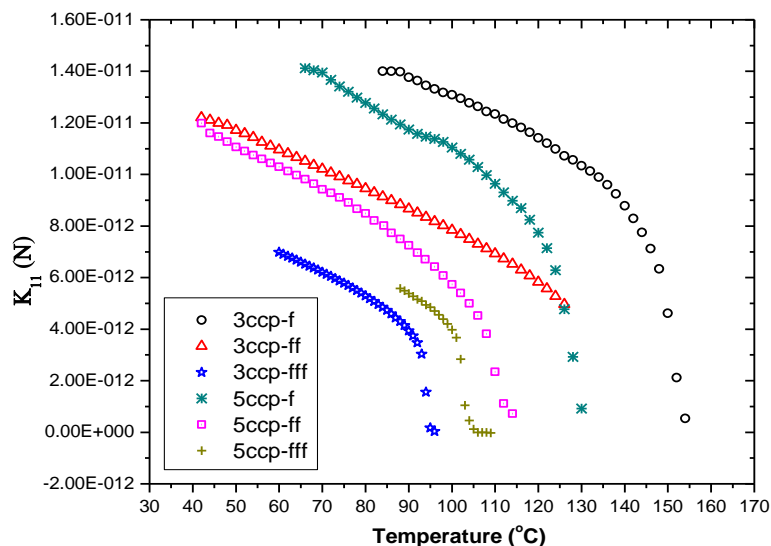
Figure 4.19: Temperature variation of splay elastic constant (K_{11}) of the compounds

Effective value of the dipole moment in nematic phase for all the six compounds were calculated following Bordewijk theory [70] of anisotropic dielectrics as detailed in chapter 2 and found to be 1.82D, 2.96D, 3.50D, 1.83D, 2.95D and 3.56D for 3ccp-f, 3ccp-ff, 3ccp-fff, 5ccp-f, 5ccp-ff and 5ccp-fff respectively whereas free molecule dipole moments were 1.93D, 3.21D, 3.72D, 1.93D, 3.12D and 3.77D respectively (Table 4.4 and 4.11). Smaller values of dipole moments within nematic phase suggest anti-parallel association of molecules. From X-ray diffraction study [24,25], it has observed that the apparent length of the molecules in nematic phase was more than the single molecular length which also suggests the presence of molecular associations. To obtain a quantitative measure of this anti-parallel correlation, dipole-dipole correlation factor g_λ has also been calculated. It is noted that $g_\lambda = 1$ signifies no correlation at all (monomeric system), $g_\lambda = 0$ means perfect antiparallel correlation and $g_\lambda = 2$ means perfect parallel correlation. The ensemble averages of the $\parallel$ and $\perp$ components of the dipole-dipole correlation factor are listed in Table 4.11.

Table 4.11: Effective values of dipole moments and dipole correlation factors

Compounds	$g_\parallel$ (near melting point)	$g_\perp$ (near melting point)	μ_{eff} (D)
3ccp-f	0.575	1.024	1.82
3ccp-ff	0.386	0.923	2.96
3ccp-fff	0.523	0.891	3.50
5ccp-f	0.479 [*]	0.976 [*]	1.83
5ccp-ff	0.488	1.028	2.95
5ccp-fff	0.473	1.119	3.56

*near SmB − N transition

Observed values of parallel correlation factor $g_\parallel$ signify weak anti-parallel correlation of the components of dipole moments along the molecular axes in nematic phase for all the compounds. Corresponding values of $g_\perp$ suggests almost no anti-parallel correlation of the perpendicular components of the dipole moments. It is further observed that, anti-parallel correlation along the molecular axis slightly improves in mono and tri fluorinated derivatives of pentyl compounds compared to propyl compounds, however in bi fluorinated derivative more correlation is observed in propyl compound.

4.4.4 Dielectric Relaxation Study

To see the dynamic response of the compounds to ac field, frequency dependent dielectric study was performed as a function of temperature. The frequency dependences of real and imaginary parts of dielectric permittivities of the six compounds are shown in Figures 4.20 − 4.25. It is clear from the figures that the real part of dielectric permittivity remains almost constant in the low temperature region (upto ~100 kHz) and decreases sharply at higher frequencies and it decreases with temperature for all the compounds. Only one strong absorption process is observed in the absorption spectra; for clarity spectra only at some selected

temperatures are presented. In each case relaxation frequencies are found to increase with temperature. Assuming the relaxation behavior is a result of Cole–Cole type process, the complex dielectric permittivity was fitted with the modified Cole-Cole equation [33] to get the actual values of relaxation frequency (*fc*) and symmetric distribution parameter (α) as detailed in chapter 2. As real and imaginary parts of dielectric constants are related through Kramers-Kronig relations, the Cole-Cole plot of the fitted spectra only at one temperature for all the six compounds are presented in Figures 4.26 – 4.31, which shows that the fitting was quite good. Nature of the absorption process is found to be almost Debye type since in no case fitted α is more than 0.05.

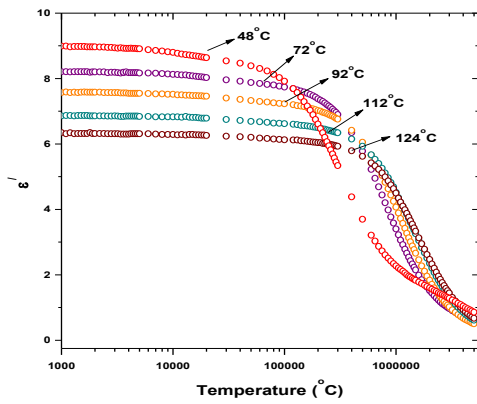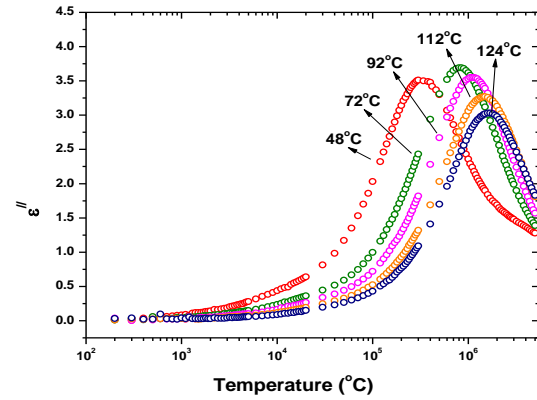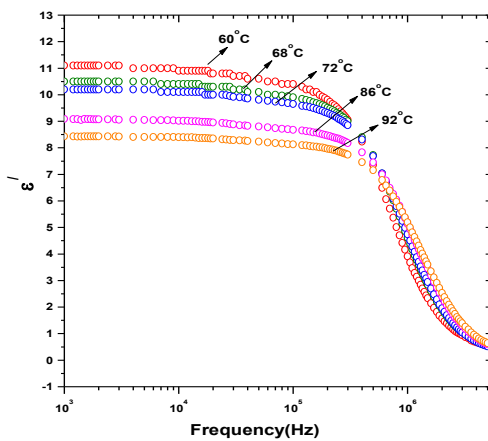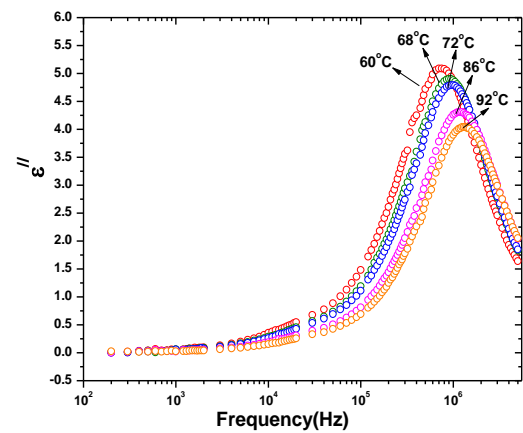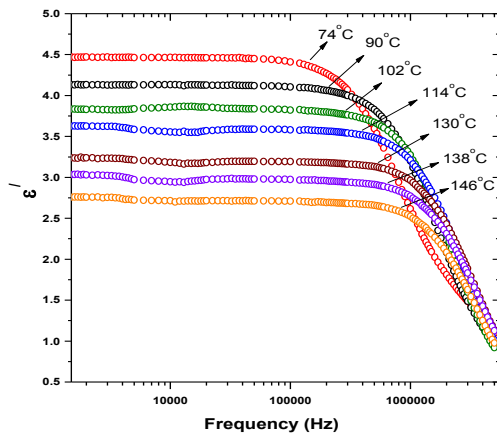(a)   (b)
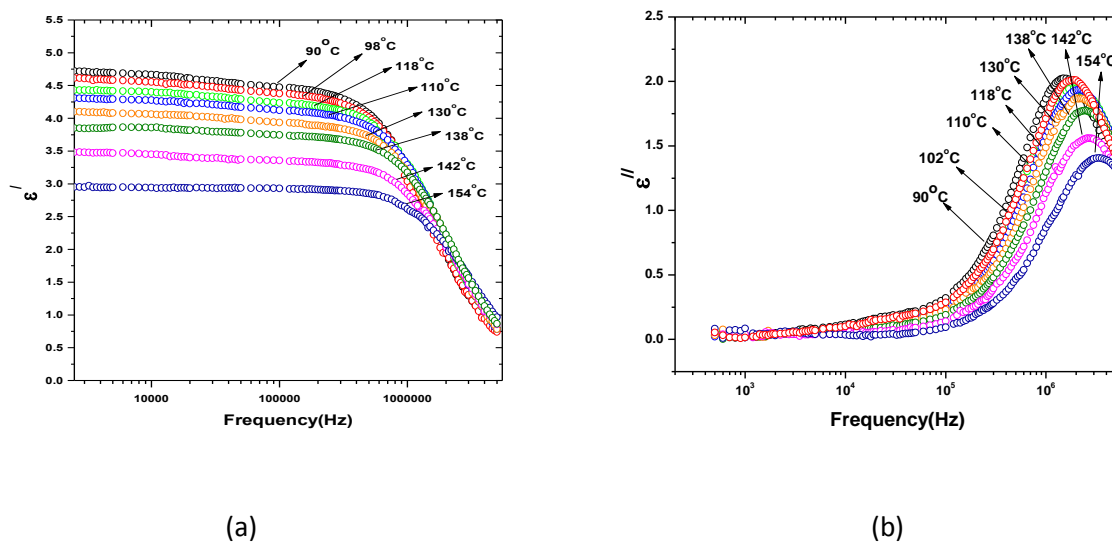
Figure 4.20: Temperature variation of (a) real and (b) imaginary part of dielectric permittivity of 3ccp-f

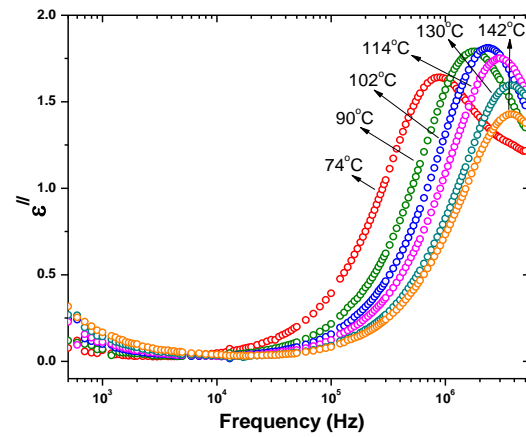Figure 4.21: Temperature variation of (a) real and (b) imaginary part of dielectric permittivity of 3ccp-ff

Figure 4.22: Temperature variation of (a) real and (b) imaginary part of dielectric permittivity of 3ccp-fff
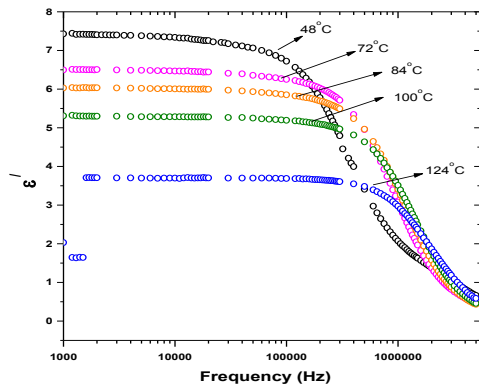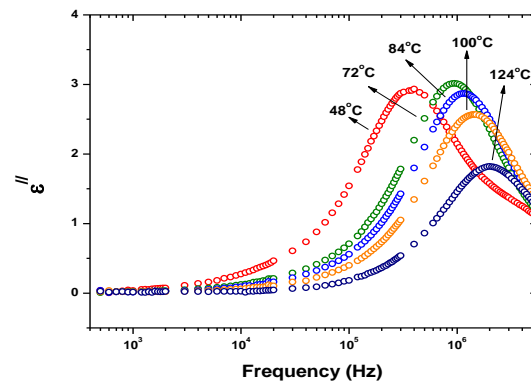
(a)

(b)

Figure 4.23: Temperature variation of (a) real and (b) imaginary part of dielectric permittivity of 5ccp-f

(a)

(b)

Figure 4.24: Temperature variation of (a) real and (b) imaginary part of dielectric permittivity of 5ccp-ff
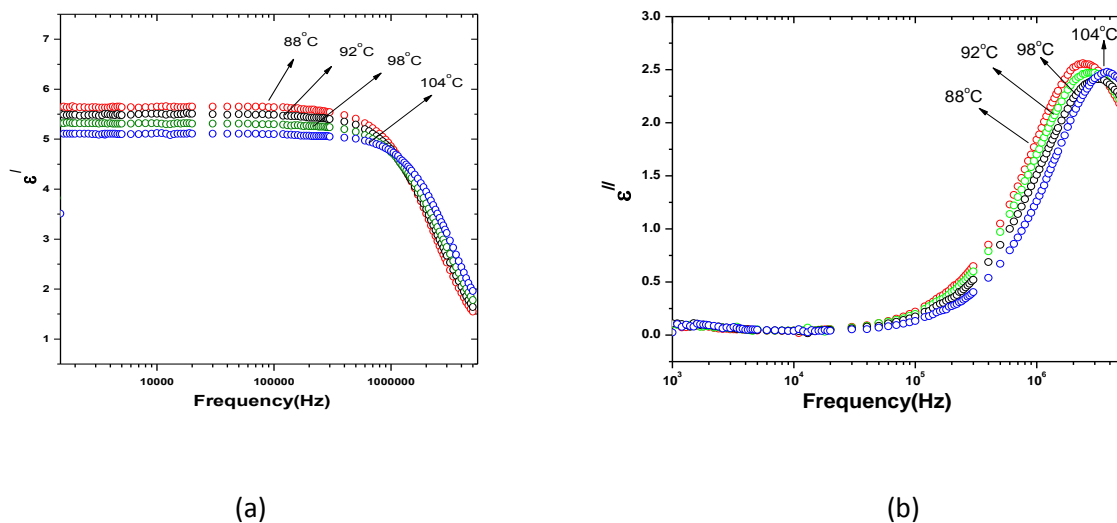
(a)   (b)

Figure 4.25: Temperature variation of (a) real and (b) imaginary part of dielectric permittivity of 5ccp-fff

Since reorientation around the long axis is usually found in GHz, observed relaxation frequencies are assumed to be associated with rotation around short molecular axis (flip-flop mode) and found to increase systematically with temperature. Observed range of relaxation frequencies of all the compounds are listed in Table 4.12.
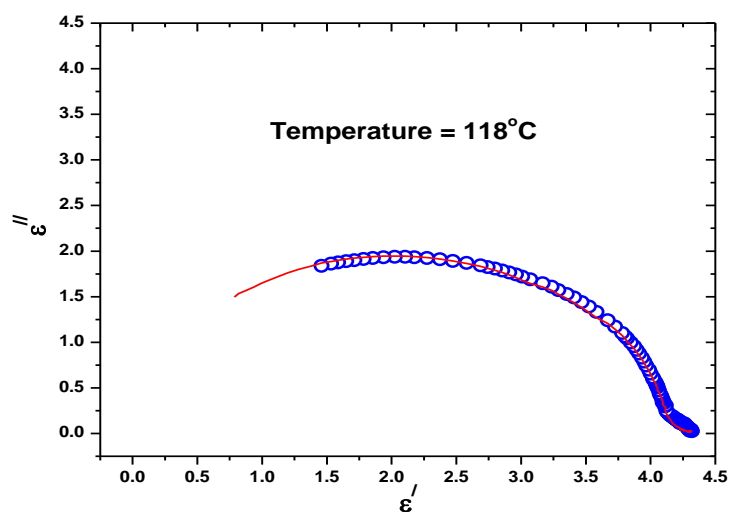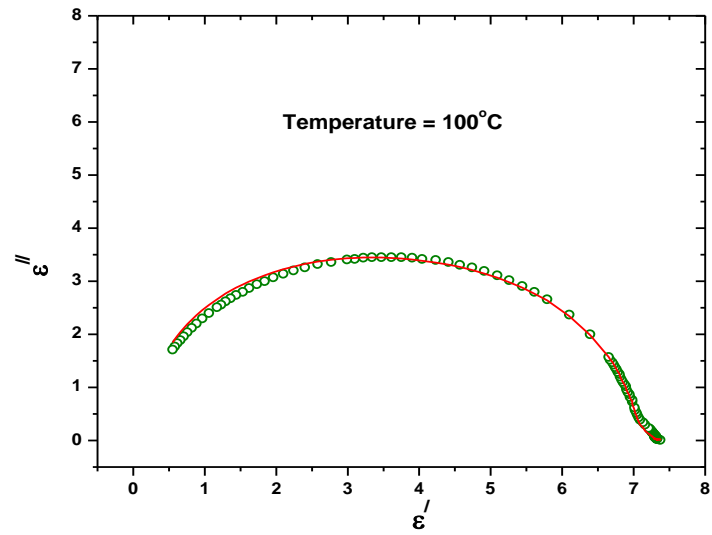

Figure 4.26: Cole-cole plot of 3ccp-f

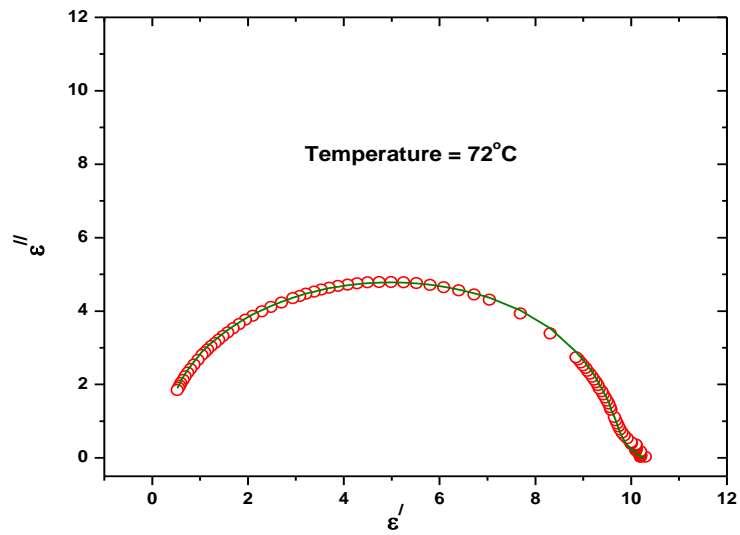Figure 4.27: Cole-cole plot of 3ccp-ff

Figure 4.28: Cole-cole plot of 3ccp-fff
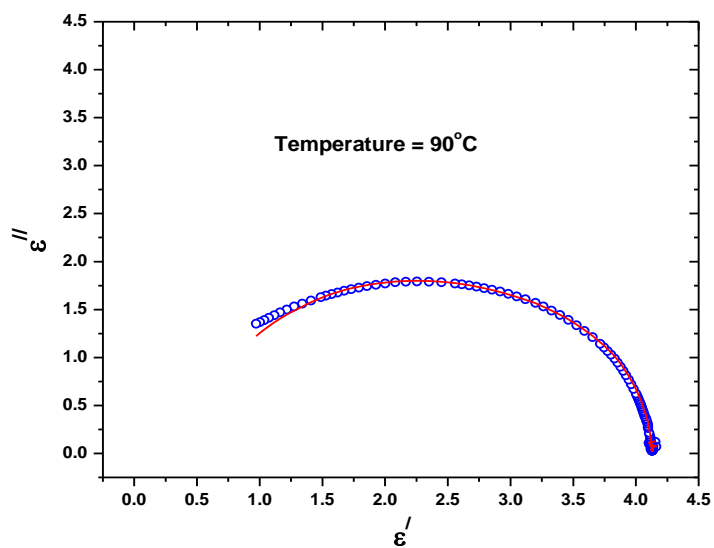
Figure 4.29: Cole-cole plot of 5ccp-f
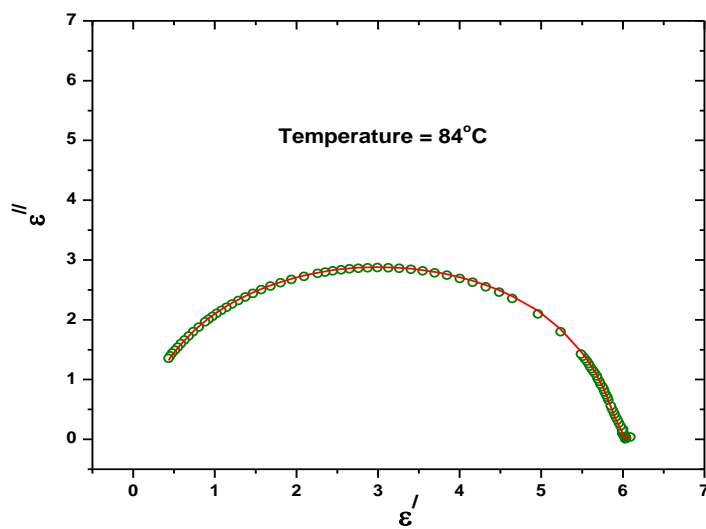
Figure 4.30: Cole-cole plot of 5ccp-ff
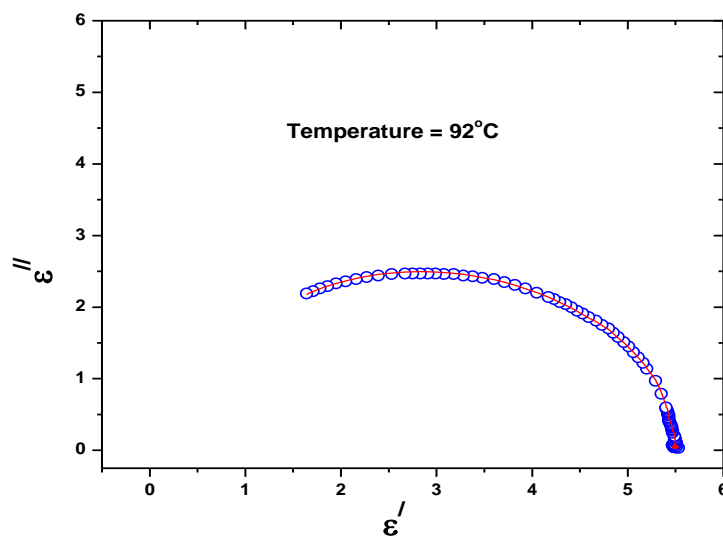
Figure 4.31: Cole-cole plot of 5ccp-fff

It is observed that for 3ccp-ff, 3ccp-fff, 5ccp-f and 5ccp-ff relaxation frequency varies from kHz regime to few MHz regimes, but for 3ccp-f and 5ccp-fff, it varies within MHz regime. In low temperature regime, relaxation frequency (f_c) decreases sharply from f to ff derivatives but increases from ff to fff derivatives in both the series. Increased chain length however, caused increased relaxation frequency except in the mono fluorinated derivatives. In terphenyl series also f_c was found to decrease with increased fluorination as noted in chapter 3. Observed values are lower than in cyanobiphenyls e.g. in 5CB it was 15.6 MHz [71]. This is expected since for rigid molecules f_c varies inversely with square root of moment of inertia [72] and present molecules have larger moments of inertia (listed in Table 4.4) mainly because of large increase in their molecular mass compared to 5CB.

Table 4.12: Relaxation frequency and activation energy of the studied compounds

Compounds	Relaxation Frequency (f_c) within nematic range	Activation Energy (kJ/mole)
3ccp-f	1.5 MHz (90°C) – 3.46 MHz (158°C)	16.14
3ccp-ff	270 kHz (45°C) – 1.78 MHz (124°C)	22.58
3ccp-fff	800 kHz (64°C) – 1.4 MHz (94°C)	20.56
5ccp-f	900 kHz (73°C) – 4.7 MHz (146°C)	29.45
5ccp-ff	400 kHz (48°C) – 2.25 MHz (128°C)	22.77
5ccp-fff	2.4 MHz (88°C) – 3.6 MHz (102°C)	32.63

Exponential increase of relaxation frequency with temperature suggests that it should obey Arrhenius law [33,73,74], following this height of the activation energy barrier of the thermally activated relaxation process was calculated and the values are listed in the Table 4.12. Activation energies of the present compounds are substantially less than the terphenyl compounds described in last chapter. These are also less than in 5CB which was reported to be 66 kJ/mole [33]. Above table also suggests that increased chain length substantially increases the activation energy in nematic phase, however, increment is marginal in ff derivatives.

It is worth of mention that the present compounds, unlike the terphenyl compounds show very low optical birefringence (Δn) in the range 0.067 to 0.034 [24,25].

4.5 CONCLUSION

Effect of fluorination and chain length on the physical properties of six phenyl bicyclohexyl compounds (3ccp-f, 3ccp-ff, 3ccp-fff, 5ccp-f, 5ccp-ff, 5ccp-fff) have been investigated, all of which exhibit nematic phase over a wide range of temperatures. Molecular mechanics calculation reveals that dipole moments of the molecules increases (1.93D to 3.37D)

with fluorination in both propyl and pentyl based systems; increment in f to ff derivatives is more than in ff to fff derivatives. However no change in dipole moment is observed with increased chain length. Molecular geometry and conformation, packing in the crystalline state and density, magnitude of molecular dipole moments and its orientation with molecular long axes of the compound 5ccp-fff is found to be different from those in closely related compounds 3ccp-f and 3ccp-fff. These differences are probably the cause of the substantial increase of melting point and decrease of nematic range in 5ccp-fff compared to compounds 3ccp-f and 3ccp-fff. The fact that in the nematic phase apparent length of the molecules is more than the most extended molecular lengths, average value of dielectric constant (ε_{avg}) is less than the extrapolated values of ε_{iso} in isotropic phase, effective values of the dipole moments are less than the free molecular dipole moments as well as calculated values of dipole-dipole correlation factors ($g_{\parallel}$ and $g_{\perp}$) give conclusive evidence of existence of short range antiparallel order in all the compounds. Antiparallel correlation ($g_{\parallel}$) along the molecular axis is found to improve slightly with increased chain length in mono and trifluorinated compounds. Increased fluoro substitution caused increased dielectric anisotropy however; increased chain length resulted in opposite behavior but in lower degree. As a result, improved switching characteristics (V_{th} and V_d) is observed in 3ccp series compared to 5ccp series and increased lateral fluorination resulted in further improvement. Increased fluorination also decreases splay elastic constant, thus faster response expected in triply fluorinated compounds. Only one Debye type relaxation process, connected with reorientations around the short axis, is observed. In low temperature regime, relaxation frequency (f_c) decreases sharply from f to ff derivatives but increases from ff to fff derivatives in both the series. Increased chain length however caused increased relaxation frequency.

4.6 REFERENCES

[1] B. Bahadur, (1991). Liquid Crystals Applications and Uses, World Sci.: Singapore.

[2] G. H. Heilmeier and L. A. Zanoni; Appl. Phys. Lett. 13, 91 (1968), Guest-host interactions in nematic liquid crystals: a new electro-optic effect.

[3] S. Marino, M. Castriota, V. Bruno, E. Cazzanelli, G. Strangi, C. Versace and N. Scaramuzza; J. Appl. Phys., 97, 013523 (2005), Changes of the electro-optic response of nematic liquid crystal cells due to inserted titania-vanadia films.

[4] M. Oh-e and K. Kondo; Appl. Phys. Lett., 69, 623 (1996), Response mechanism of nematic liquid crystals using the in-plane switching mode.

[5] R. Muenster, M. Jarasch, X. Zhuang and Y. R. Shen; Phys. Rev. Lett., 78, 42 (1997), Dye-Induced Enhancement of Optical Nonlinearity in Liquids and Liquid Crystals.

[6] Y. Goto, T. Ogawa, S. Swada and S. Sugimori; Mol. Cryst. Liq. Cryst., 209, 1–7 (1991), Fluorinated Liquid Crystals for Active Matrix Displays.

[7] D. Demus, Y. Goto, S. Sawada, E. Nakagawa, H. Saito, R. Tarao; Mol Cryst Liq Cryst., 260, 1–21(1995), Trifluorinated liquid crystals for TFT displays.

[8] T. Nishi, A. Matsubara, H. Okada, H. Onnagawa, S. Sugimori, K. Miyashita; Jpn J Appl Phys., 34, 236–239 (1995), Relationship between molecular structure and temperature dependence of threshold voltage in fluorinated liquid crystals.

[9] V. F. Petrov; Liq Cryst., 19, 729–741 (1995), Liquid crystals for AMLCD and TFTPDLCD applications; V. F. Petrov, Sofia I. Torgova ; Ludmila A. Karamysheva ; Shunsuke Takenaka; Liq. Cryst., 26, 1141-1162 (1999), The trans-1,4-cyclohexylene group as a structural fragment in liquid crystals.

[10] S. Gauza, H. Wang, C. H. Wen, S. T. Wu, A. Seed, R. Dabrowski; Jpn J Appl Phys., 42, 3463–3466 (2003), High birefringence isothiocyanato tolane liquid crystals.

[11] J. S. Gasowska, S. J. Cowling, M. C. R. Cockett, M. Hird, R. A. Lewis, E. P. Raynes, J. W. Goodby; Mater Chem., 20, 299–307 (2010), The influence of an alkenyl terminal group on the mesomorphic behavior and electro-optic properties of fluorinated terphenyl liquid crystals.

[12] H. Ishikawa, A. Toda, H. Okada, H. Onnagawa, S. Sugimori; Liq Cryst., 22, 743–747 (1997), Relationship between order parameter and physical constants in fluorinated liquid crystals.

[13] M. Hird; Chem Soc Rev., 36, 2070–2095 (2007), Fluorinated liquid crystals – properties and applications.

[14] M. Klasen, M. Bremer, A. Gotz, A. Manabe, S. Naemura, K. Tarumi; Jpn J Appl Phys., 37, L945–L948 (1998), Calculation of optical and dielectric anisotropy of nematic liquid crystals.

[15] K. Hori, M. Maeda, M. Yano, M. Kunugi; Liq Cryst., 38, 287–293 (2011), The effect of fluorination (2): dependence of alkyl chain length on the crystal structures of mesogenic alkyl 4-[2-(perfluorohexyl) ethoxy] benzoates.

[16] M. R. Cargill, G. Sandford, A. J. Tadeusiak, G. D. Love, N. Hollfelder, F. Pleis, G. Nelles, P. Kilickiran; Liq Cryst., 38, 1069–1078 (2011), Highly fluorinated biphenyl ether systems as dopants for fastresponse liquid crystal display applications.

[17] S. Haldar, K. C. Dey, D. Sinha, P. K. Mandal, W. Haase, P. Kula; Liq Cryst., 39, 1196–1203 (2012), X-ray diffraction and dielectric spectroscopy studies on a partially fluorinated ferroelectric liquid crystal from the family of terphenyl esters.

[18] E. Bartmann, D. Dorsch, U. Finkenzeller, H. A. Kurmeier and E. Poetsch; Freiburger Arbeitstagung Flüssigkristalle, 19, P8 (1990).

[19] U. Finkenzeller, A. Kurmeier and E. Poetsch; Freiburger Arbeitstagung Flüssigkristalle, 18, P17 (1989).

[20] P. Kirsch, S. Naemura and K. Tarumi; Freiburger Arbeitstagung Flüssigkristalle, 27, P45 (1998).

[21] K. Tabayashi and K. Akasaka; Liq. Cryst., 26, 127-129 (1999), Preliminary communication Natural abundance 2H NMR for liquid crystal studies: deuterium isotope effect on microscopic order.

[22] H. Ishikawa, A. Toda, A. Matsubara, T. Nishi, H. Okada, H. Onnagawa, S. Sugimori and K. Miyashita; 20th Jpn. Symp. Liq. Cryst., Nagoya 1G505 (1994).

[23] D. A. Dunmur, R. Hanson, H. Okada, H. Onnagawa, S. Sugimori and K. Toriyama; Asia Display' 95Proceeding, S22-2, 563 (1995), Effect of Intermolecular Interactions on Threshold Voltages for TN and TFT LC-Displays: Dipole Association in F-Substituted Cyclohexyl cyclohexyl benzenes.

[24] S. Biswas, S. Haldar, P. K. Mandal, W. Haase; Liq Cryst., 34, 365–372 (2007), X-ray diffraction and optical birefringence studies on four nematogenic difluorobenzene derivatives.

[25] S. Haldar, S. Barman, P. K. Mandal, W. Haase, R. Dabrowski; Mol Cryst Liq Cryst.,528, 81–95 (2010), Influence of molecular core structure and chain length on the physical properties of nematogenic fluorobenzene derivatives.

[26] I. C. Khoo and S. T. Wu; Optics and Nonlinear Optics of Liquid Crystals, World Scientific: Singapore, (1993).

[27] L. M. Blinov, V. G. Chigrinov; Electro-Optic Effects in Liquid Crystal Materials, Springer: New York, (1996).

[28] M. Schadt; Annu. Rev. Mater. Sci., 27, 305–379 (1997), Liquid crystal materials and liquid crystal displays.

[29] B. Kundu, S. K. Pal, S. Kumar, R. Pratibha, N. V. Madhusudana; Phys Rev E., 82, 061703-1–061703-9 (2010), Splay and bend elastic constants in the nematic phase of some disulfide bridged dimeric compounds.

[30] H. Kresse; Dynamic dielectric properties of nematics. In: Dunmur, DA. Fukuda, A. Luckhurst, GR, editors. Physical properties of liquid crystals: nematics. London: INSPEC; 2001. p. 277–287.

[31] H. Kresse; Dielectric properties of nematic liquid crystals. In: Demus, D. Goodby, J. Gray, GW. Spiess HW. Vill, V, editors. Handbook of liquid crystals. Vol. 2A. Weinheim, FRG: Wiley-VCH, Verlag GmbH, p. 91–112 (1998).

[32] W. H. de Jeu, T. W. Lathouwers, D. Constants; ZNaturforsch, 29a, 905–911 (1974), Molecules structure of nematic liquid crystals. I. Terminally substituted azobenzene and azoxybenzenes.

[33] J. Schacht, P. Zugenmaier, M. Buivydas, L. Komitov, B. Stebler, S. T. Lagerwall, F. Gouda, F. Horii; Phys Rev E., 61, 3926–3935 (2000), Intermolecular and intramolecular reorientations in nonchiral smectic liquid-crystalline phases studied by broadband dielectric spectroscopy.

[34] D. A. Dunmur, W. H. Miller; Mol Cryst Liq Cryst., 60, 281–292 (1980), Dipole–Dipole correlation in nematic liquid crystals.

[35] S. Haldar, D. Sinha, P. K. Mandal, K. Goubitz and R. Peschar; Liquid Crystals, Vol. 40, No. 5, 689–698 (2013), Effect of molecular conformation on the mesogenic properties of a partially fluorinated nematogenic compound investigated by X-ray diffraction and dielectric measurements.

[36] S. Haldar, P. K. Mandal, K. Goubitz, H. Schenk, W. Haase; Mol Cryst Liq Cryst., 490, 80-87 (2008), X-ray structural analysis in the crystalline phase of a nematogenic fluoro-phenyl compound.

[37] S. Haldar, P. K. Mandal, S. J. Prathap, T. N. Guru Row, W. Haase; Liq Cryst., 35, 1307–1312 (2008), X-ray studies of the crystalline and nematic phases of 4_-(3,4,5-trifluorophenyl)-4-propylbicyclohexyl.

[38] W. Haase, M. A. Athanassopoulou; Vol. I. Berlin: Springer, p. 139–197 (1999), Crystal structures of LC mesogens. In: Mingos, M, editor. Structure and bonding.

[39] M. Hird and K. J. Toyne; Mol. Cryst. Liq. Cryst., 323, 1-67 (1998), Fluoro Substitution inThermotropic Liquid Crystals.

[40] V. Vill; Liq. Cryst. Database, Version 4.4 , LCI Publisher, GmbH, Hamburg (2003) and references therein.

[41] L. Bata and A. Buka; Mol. Cryst. Liq. Cryst, 63, 307-320 (1981), Dielecteric Permittivity and Relaxation Phenomena in smectic Phases.

[42] R. deGelder, R. A. G. de Graaff, H. Schenk; Acta Cryst., A49, 287−293 (1993), Automatic determination of crystal structures using Karle-Hauptman matrices.

[43] D. T. Cromer, J. B. Mann; Acta Cryst., 24A, 321−324 (1968), X-ray scattering factors computed from numerical Hartree–Fock wave functions.

[44] International Union of Crystallography. International tables for X-ray crystallography. Vol. IV, Birmingham: Kynoch Press, pp. 55 (1974).

[45] D. T. Cromer, D. Liberman; J Chem Phys., 53, 1891−1898 (1970), Relativistic calculation of anomalous scattering factors for X-rays.

[46] S. R. Hall, D. J. du Boulay, R. Olthof-Hazekamp, editors. XTAL3.7 system. Lamb: University of Western Australia (2000).

[47] Spek AL. PLATON, An integrated tool for the analysis of the results of a single crystal structure determination. Acta Cryst., A46, C−34 (1990).

[48] Hyperchem 6.03, Hypercube Inc., Gainesville, FL, USA.

[49] P. Sarkar, P. K. Mandal, S. Paul, R. Paul; liq. Cryst, Vol. 30, No. 4, 507−527 (2003), X-ray diffraction, optical birefringence, dielectric and phase transition properties of the long homologous series of nematogens 4-(trans-4∞-n-alkylcyclohexyl) isothiocyanatobenzenes.

[50] E. Megnassan and A. Proutierre; Mol. Cryst. liq. Cryst., 108, 245 (1984), Dipole Moments and Kerr Constants of 4-n Alkyl-4′- Cyanobiphenyl Molecules (From 1CB to 12CB) Measured in Cyclohexane Solutions.

[51] K. P. Gueu, E. Megnassan and A. Proutierre; Mol. Cryst. liq. Cryst., 132, 303 (1986), Dipole Moments of 4-n Alkyl-4′-Cyanobiphenyl Molecules (from OCB to 12CB) Measurement in Four Solvents and Theoretical Calculations.

[52] W. Haase, H. Paulus, R. Pendzialek; Mol. Cryst. Liq. Cryst., 100: 211-221 (1983), Solid State Polymorphism in 4-Cyano-4′-n-Propyl biphenyl and X-Ray Structure Determination of the Higher Melting Modification.

[53] B. R. Jaishi, P. K. Mandal, K. Goubitz, H. Schenk, R. Dabrowski, K. Czuprynski; Liq.Cryst., 30, 1327-1333 (2003), The molecular and crystal structure of a polar mesogen 4-cyanobiphenyl-4′-hexylbiphenyl carboxylate.

[54] S. Biswas, S. Haldar, P. K. Mandal, K. Goubitz, H. Schenk, R. Dabrowski; Cryst. Res. Technol., 42, 1029-1035 (2007), Crystal structure of a polar nematogen 4-(trans-4-undecylcyclohexyl) isothiocyanatobenzene.

[55] L. Walz, W. Haase, R. Eidenschink; Mol. Cryst. Liq. Cryst., 168, 169-182 (1989), The Crystal and Molecular Structures of Four Homologous, Mesogenic trans,trans-4,4'-dialkyl-(1α,1'-bicyclohexyl)-4β-carbonitril (CCN's).

[56] S. Gupta, P. Mandal, S. Paul, K. Goubitz, M. de Wit, H. Schenk; Mol. Cryst. Liq.Cryst., 195, 149-159 (1991), An X-Ray Study of Cyanophenylpyrimidines Part III. Crystal Structure of 5-(trans-4-Heptylcyclohexyl)-2-(4-Cyanophenyl) Pyrimidine.

[57] A. Nath, S. Gupta, P. Mandal, S. Paul, H. Schenk; Liq. Cryst., 20, 765-770 (1996), Structural analysis by X-ray diffraction of a non-polar alkenyl liquid crystalline compound.

[58] P. Mandal, S. Paul, H. Schenk, K. Goubitz; Mol. Cryst. Liq. Cryst., 210: 21-30 (1992), Crystal and Molecular Structure of a Cybotactic Nematic Compound bis-(4′-n-Butoxybenzal)-2-Chloro-l,4-Phenylinediamine.

[59] P. Mandal, S. Paul, H. Schenk, K. Goubitz; Mol. Cryst. Liq. Cryst., 135, 35-48 (1986), Crystal and Molecular Structure of the Nematogenic Compound 4-Cyanophenyl-4'-n-Heptylbenzoate (CPHB).

[60] P. Mandal, S. Paul; Mol. Cryst. Liq. Cryst., 131, 223-235 (1985), X-Ray Studies on the Mesogen 4'-n-Pentyloxy-4-Biphenylcarbonitrile (5OCB) in the Solid Crystalline State.

[61] L. Walz, F. Nepveu, W. Haase; Mol. Cryst. Liq. Cryst., 148, 111-121 (1987), Structural Arrangements of the Mesogenic Compounds 4-Ethyl-4′-(4″-pentylcyclohexyl)biphenyl and 4-Ethyl-2′-fluoro-4′-(4″-pentylcyclohexy1)biphenyl (BCH's) in the Crystalline State.

[62] P. S. Patil, V. Shettigar, S. M. Dharmaprakash, S. Naveen, M. A. Sridhar, J. S. Prasad; Mol. Cryst. Liq. Cryst., 461, 123-130 (2007), Synthesis and Crystal Structure of 1-(4-fluorophenyl)-3-(3,4,5-trimethoxyphenyl)-2-propen-1-one.

[63] S. Haldar; S. Barman; P. K. Mandal; W. Haase; R. Dabrowski; Mol. Cryst. Liq. Cryst., Vol. 528, 81–95 (2010), Influence of Molecular Core Structure and Chain Length on the Physical Properties of Nematogenic Fluorobenzene Derivatives.

[64] A. J. Leadbetter, R. M. Richardson, C. N. Colling; 36, C1-37–C1-43 (1975), The structure of a number of nematogens. J Phys (Paris).

[65] S. Gupta, G-P Chang-Chien, W-S Lee, R. Centore, S. P. Sen Gupta; Liq Cryst., 29, 657–661 (2002), Crystal structure of the mesogenic alkene monomer, 3-[4-(4_-ethylbiphenyl)]-1-propene.

[66] B. R. Ratna, R. Shashidhar; Mol Cryst Liq Cryst., 42, 113–125 (1977), Dielectric studies on liquid crystals of strongly positive dielectric anisotropy.

[67] B. R. Ratna, R. Shashidhar; Mol Cryst Liq Cryst., 45, 103–116 (1978), Dielectric properties of some nematics of positive dielectric anisotropy.

[68] M. Schadt; J Chem Phys., 56, 1494–1497 (1972), Dielectric properties of some nematic liquid crystals with strong positive dielectric anisotropy.

[69] N. V. Madhusudana, S. Chandrasekhar; Pramana., 1, 57–68 (1975), The role of permanent dipoles in nematic order.

[70] P. Bordewijk; Physica., 75, 146 (1974), Extension of the Kirkwood-Fröhlich theory of the static dielectric permittivity to anisotropic liquids.

[71] M. Gu, Y. Yin, S. V. Shiyanovskii, O. D. Lavrentovich; Phys Rev E., 76, 061702 (2007), Effects of dielectric relaxation on the director dynamics of uniaxial nematic liquid crystals.

[72] H. Baessler, R. B. Beard, M. M. Labes; J Chem Phys., 52, 2292 (1970), Dipole Relaxation in a Liquid Crystal.

[73] A. C. Diogo, A. F. Martins; J Phys (Paris), 43, 779 (1982), Order parameter and temperature dependence of the hydrodynamic viscosities of nematic liquid crystals.

[74] S. Arrhenius; Z Phys Chem., 4, 226 (1889), On the reaction rate of the inversion of non-refined sugar upon souring.